AIChE WILEY InterScience DISCOVER SOMETHING GREAT

PARTICLE TECHNOLOGY AND FLUIDIZATION

Monitoring a Crystallization Induced by Compressed CO_2 with Raman Spectroscopy

Arlette Vega-González, Philippe Marteau, and Pascale Subra-Paternault
Laboratoire d'Ingénierie des Matériaux et des Hautes Pressions (LIMHP), CNRS, Institut Galilée, Université Paris 13, 93430 Villetaneuse, France

DOI 10.1002/aic.10740
Published online December 5, 2005 in Wiley InterScience (www.interscience.wiley.com).

The application of on-line Raman spectroscopy for detecting and monitoring a CO_2 antisolvent process (GAS) is explored for the first time. Griseofulvin precipitations were carried out in a batch vessel from an acetone liquor, in which the CO_2 was introduced at specific rates. Changes of griseofulvin and acetone concentrations upon addition of CO_2 were monitored through specific wavenumbers at different pressurization rates (0.10 and 0.45 MPa/min) and courses (continuous or stepwise introduction, final pressure of 10 or 4.8 MPa). The ratio between the solute and solvent signals allowed for accurately detecting the onset of crystallization, for monitoring the depletion of the solution in solute as a function of time, and for estimating the mass of precipitated solids during the crystallization course. Moreover, the Raman spectroscopy provided experimental evidence of the predicted scenario of a crystallization induced by supercritical fluid. © 2005 American Institute of Chemical Engineers *AIChE J,* 52: 1308–1317, 2006
Keywords: crystallization, Raman spectroscopy, supercritical carbon dioxide, on-line monitoring, antisolvent

Introduction

In the pharmaceutical industry, the manufacturing of tablets or capsules (which represents the major part of pharmaceutical products) is largely dominated by powder technology. Indeed, most of the manufacturing operations (that is, crystallization/drying, milling, blending, granulation, encapsulation, tableting, etc.) are devoted to making particles, modifying their properties, and turning them into structured products. Although most of the operations have benefited from enhanced scientific attention, crystallization is perhaps the area that has witnessed the greatest progress in the past few years.[1] One reason is that the method for producing the drug is a critical step in the final product performances, given that crystal habit and crystal size distribution play a large role in the therapeutic behavior. The development of effective particle technologies is keeping up with the need for increasingly smaller crystals of increased purity, which allow reduction of the drug dosage while retaining the therapeutic benefits, and minimize the side effects. Crystallization using supercritical fluids (SCFs) was mostly developed as an alternative approach to conventional liquid crystallization, with aims of controlling the particle size and reducing the residual solvent concentration in drugs, besides the environmental advantage of reducing the liquid solvent wastes.

During the last decade, SCF technology has been applied to several operations involved in the pharmaceutical manufacturing area, such as crystallization,[2] drying,[3] coating,[4] or blending,[5] to improve the physical and chemical properties of the drug products and their interactions with the biological environment. Although many fluids could be chosen for crystallization purposes, carbon dioxide (SC-CO_2) is by far the most extensively used when processing pharmaceutical compounds. The reasons mostly rely on CO_2's mild critical conditions of temperature (T_c = 31.05°C) and pressure (P_c = 7.28 MPa) that allow for processing temperature– or shear-sensitive drugs, and its nontoxic, nonflammable, inert, and cheap characteristics. In SCF-crystallization techniques, the SCF can act as a solvent or

Correspondence concerning this article should be addressed to P. Subra-Paternault at subra@limhp.univ-paris13.fr.

as a precipitating agent, that is, an antisolvent. In this latter technique, the compound of interest is first dissolved in an organic solvent. The addition of CO_2 to that liquor solution decreases the solvation ability of the original solvent and causes precipitation of the solute.

Crystallization by addition of a liquid antisolvent is widely used in the chemical, food, and pharmaceutical industries, especially as a batch operation.[6] Because many pharmaceutical crystallization processes have been designed mostly by empiricism,[1] there is a need for on-line process monitoring and control.[7] Spectroscopic methods have gained popularity during the last years in the crystallization field. For instance, these techniques were used recently to determine the onset of crystallization by UV/visible (UV-vis) and fluorescence spectroscopy,[8,9] for particle size measurements by ultrasonic spectroscopy,[10] to obtain information on the kinetics of polymorphic transitions with near-infrared spectroscopy,[11] and to determine concentration/supersaturation profiles[12-19] and solubility curves[14,15,19,20] with Raman[13,14,20] and attenuated total reflection (ATR) FTIR[12,15-19] spectroscopies. These examples deal with batch crystallization processes run at atmospheric pressure; for most of them, crystallization was induced by cooling the liquor, whereas only few applied to antisolvent crystallization.

Crystallization induced by supercritical CO_2 as nonsolvent is gaining importance, although pressurized vessels actually hinder in situ monitoring of the crystallization course. Spectroscopic investigations to monitor crystallization induced by compressed fluids from a solution are scarce. UV-vis spectroscopy was proposed to investigate the precipitation kinetics of a biodegradable polymer by compressed CO_2.[21] The UV spectrometer was linked to a high-pressure cell of 8 mL, in which 3 mL of the polymer–methylene chloride solution was introduced. Experiments were performed in the batch mode, that is, with a subsequent addition of CO_2 at various rates ranging from 0.013 to 0.08 MPa/min. The attenuation of light arising from the scattering of the suspended particles was monitored during the precipitation process by measuring the absorbance of a monochromatic beam at a wavelength of 600 nm. Thus, the UV-vis spectrometer measured the slurry turbidity generated by the polymer precipitation and subsequent formation of particles. To understand and characterize the precipitation behavior, a model based on a population balance was developed, taking into account nucleation, growth, aggregation, and settling phenomena. The absorbance measurements were related to the second moment of the simulated particle size distribution, and the kinetic parameters were thus estimated based on spectroscopic data. The experimental setup with UV spectroscopy was clearly suitable to follow accurately the time course of precipitation under pressure.

The objective of the work is to develop a non-invasive spectroscopy to monitor a crystallization process in pressurized medium, at scale and conditions representative for industrial perspectives. The Raman spectroscopy was proposed because of its ability to monitor the individual concentration of each component involved in the crystallization process—that is, the solute, the solvent, and CO_2—through the selection of specific wavenumbers and spectra calibrations. This first set of experiments aims at validating the spectroscopic technique to the detection of the precipitation onset and to the monitoring of the crystallization course under various experimental conditions.

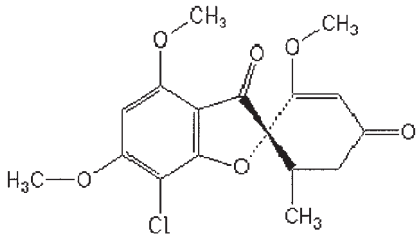

Figure 1. Structure of griseofulvin.

Raman spectroscopy also enabled us to analyze the phase behavior involved during the CO_2 addition and the monitoring of the solvent removal during the washing and drying of produced crystals, data that are not outlined here.

Griseofulvin was chosen as a model solute because of previous investigations on its precipitation by CO_2[22] and on phase equilibria as well.[23] These investigations highlighted the antisolvent effect of CO_2 when added to an acetone liquor, based on the decrease of the equilibrium concentration of griseofulvin with the enrichment of the mixture in CO_2. Griseofulvin, an oral antifungal agent, shows a very low aqueous solubility and a slow dissolution rate that induce a slow, erratic, and incomplete absorption from the gastrointestinal tract.[24] It is expected that successful micronization in small particles would improve its dissolution behavior. The component structure is given in Figure 1.

Antisolvent Crystallization

The fundamental driving force for crystallization is the difference in chemical potential between supersaturated and saturated solutions. The chemical potential difference is generally expressed as a function of the supersaturation S, defined as the ratio between the solute concentration in the solution C and the equilibrium concentration (solubility) C_s at a given temperature and pressure. Strictly speaking, the potential difference should be expressed as a function of solute activity (related to concentration through the corresponding activity coefficient) rather than concentration. The two expressions are equivalent when deviation from an ideal solution is negligible, that is, at infinite dilution or, for a nonelectrolyte solute, at concentrations < 0.1 mol/L.[6] Griseofulvin is a nonelectrolyte, and initial solutions were prepared at concentrations of 0.069 mol/L. The use of supersaturation as a measure of the thermodynamic driving force is thus satisfactory, especially for a general description of the path of a CO_2 crystallization process for which no data are available.

Supersaturation may be created by various methods that regulate either the solute concentration C or the solute solubility C_s. In antisolvent crystallization, the solution becomes supersaturated by the addition of a substance that reduces the solubility of the solute in the initial solvent. As a result of the mixing of the antisolvent and the solvent, the solute concentration also decreases by simple dilution. Figure 2 shows the qualitative evolution of the system in case of the recrystallization of griseofulvin induced by the addition of CO_2 to an acetone liquor. Two lines are drawn: the equilibrium line $C_s = f(X_{CO2})$ and the metastable line $C^* = f(X_{CO2})$. The equilibrium line, expressed as a molar fraction of solute in the acetone–CO_2 mixture, was experimentally determined at 39°C

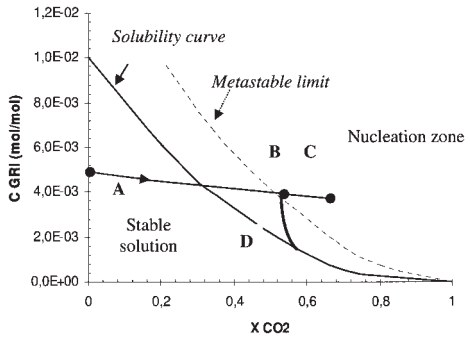

Figure 2. Qualitative evolution of the system during the recrystallization of griseofulvin from acetone induced by addition of CO_2 as antisolvent.

The solubility curve, expressed as molar fraction of the solute in acetone–CO_2 mixture, was experimentally determined[23] at $T = 39°C$ and $P = 10$ MPa, whereas the metastable line is hypothetical. The molar fraction X_{CO2} refers to the CO_2 content in the acetone–CO_2 mixture.

and 10 MPa[23]; the metastable line is hypothetical. The antisolvent crystallization proceeds first by dissolving the solute in an organic solvent, giving a concentration C_0 that is represented in Figure 2 by point A. To generate crystals, the representative point has to move from that monophasic stable domain up to the metastable boundary (point B) or beyond (point C). With a concentration expressed as molar fraction, the representative trajectory is not horizontal because the addition of CO_2 affects the total mole number of the acetone–CO_2 medium. At point B or C, the supersaturation S^* is large enough for nucleation to occur spontaneously, but growth is also significant. For high S values, nucleation will largely prevail over growth, and the zone is thus termed as catastrophic nucleation zone. To avoid further generation of new particles during the growth of older ones, which should broaden the particle size distribution (PSD), the system must be brought back quickly into the metastability domain. Nucleation is thus stopped and crystal growth is the main mechanism that allows the system to recover an equilibrium state (point D). Trajectories of the representative points depend of the antisolvent flux (horizontal component of the representative point velocity) and upon nucleation and growth rates (vertical component of the velocity). The final PSD is mainly controlled by the residence time of the system beyond and within the metastable zone.[25] Residence time in the nucleation and growth area (beyond the metastable limit) gives the width of the PSD, whereas the average size of the PSD is a function of the residence time in the growth zone, that is, within the metastable zone, in which only the growth rate is significant.

In many batch supercritical processes, the addition of CO_2 continues until a desired pressure is attained, given that nonwindowed vessels preclude the detection of the crystallization onset. The representation point of such process operates close to or above the metastable limit, especially if the feed rate of CO_2 is high. The system could cross the metastable line several times, depending on the relative rates of supersaturation buildup by the CO_2 addition rate and the depletion of solute by the growth rate. Consequently, several nucleation bursts may occur that, combined with the growth of the several bursts of nuclei, would result in a large final PSD. Conversely, if the addition rate of CO_2 is so slow that it enables the system to operate back to the equilibrium curve once the few nuclei appear, one can expect larger crystals with a narrow PSD.[26]

With compressed antisolvent, the situation is complicated by the fact that equilibrium and metastable lines vary with pressure. In a discontinuous process, the CO_2 addition provokes an increase of the pressure, given that the composition of the newly formed CO_2–solvent mixture evolves as well. Strictly speaking, the representative trajectory of a discontinuous crystallization should be considered in a three-dimensional plot, with CO_2 content and pressure as x-axis and y-axis, respectively. Although qualitative, Figure 2 nonetheless provides a suitable framework to understand the scenario of a crystallization course induced by CO_2.

Experimental

Materials

Carbon dioxide was purchased from Air Liquide (99.5% purity). Acetone (RP, 99.8% purity) and griseofulvin (minimum 95% purity) were provided by Sigma Aldrich. Griseofulvin (GRI) was stored at −18°C, and fresh solutions were prepared for immediate use.

Apparatus

Experiments were carried out in a high-pressure, optically accessible vessel that operated in a batch mode (Figure 3). The experimental system and procedure are discussed only briefly because additional details can be found elsewhere.[22] The crystallizer was a stainless steel vessel of 0.491 L (Top Industrie, France; internal diameter of 5 cm), equipped with three sapphire windows and an electric motorized stirrer. The agitator was an eight-bladed impeller of 2.5 cm in diameter, distant by 85 mm from the vessel bottom. A stainless steel frit of 2 μm in porosity was located at the vessel bottom to collect produced

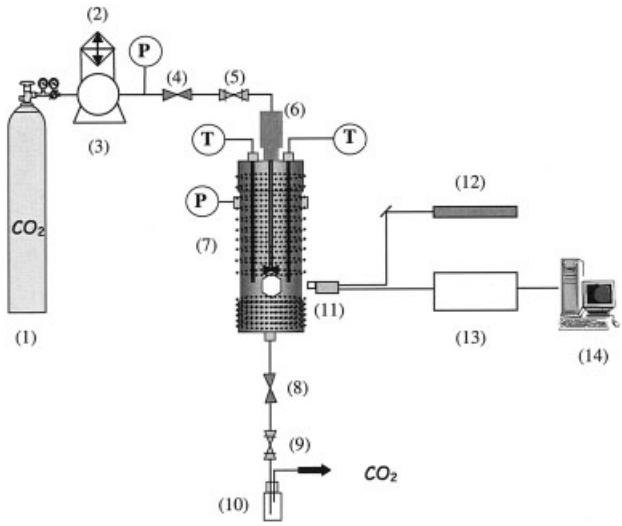

Figure 3. Experimental setup for the batch crystallization induced by addition of carbon dioxide.

Legend: (1) CO_2 cylinder; (2) chiller; (3) CO_2 pump; (4; 8) stop valve; (5, 9) metering valve; (6) stirrer; (7) crystallizer; (10) solution collector; (11) probe head; (12) argon-ion laser; (13) Raman spectrometer; (14) computer.

crystals. At the exit, a shutoff valve and a metering valve (Autoclave Engineers) allowed discharge of the solution and regulated the vessel pressure during the final steps. The exit lines were heated to avoid solidification of CO_2. The operating temperature was measured by a type K thermocouple with an accuracy of 1°C and was controlled by electric resistances. Pressures of the vessel and of the CO_2 feed line were measured by pressure sensors (Asco) with an accuracy of 0.1 MPa. The CO_2, cooled by a chiller, was delivered through the impeller by a high-pressure pump (Lewa).

Raman instrumentation

Crystallization was monitored by *noninvasive* Raman spectroscopy with a Dilor (Induram) spectrometer equipped with a CCD camera detector. The range of wavenumbers selected for the study was 750–1770 cm^{-1} because this region contained accessible griseofulvin, acetone, and CO_2 vibrational bands. The use of a 1200 lines/mm grating and a focal length of 600 mm allows scanning of the spectral range without any rotation of the grating. Excitation light at 514.53 nm was obtained from a Coherent argon-ion laser, operating at a power of 250 mW. The instrument grating was calibrated using neon lines. Remote Raman measurements were performed through a probe head (Dilor superhead), equipped with interferential and notch filters, and connected to the laser and the spectrometer by two optical fibers of 100 μm core and 5 m long. The probe head, working in the backscattered mode, was positioned directly in front of one sapphire window of the vessel. Thus, the crystallization medium was not disturbed by any immersed probe. The standard focusing objective of 40 mm focal length was replaced by a lens of 80 mm focal length to focus the incident laser beam at the center of the vessel, in the radial direction. To prevent any damage of the filters, excitation power at the sample level was limited to about 40 mW.

Each spectrum was a sum of ten accumulations collected over 10 s each (for a total spectra acquisition time of 100 s), except during Run 4, in which spectra were acquired in only 10 s to keep up with the high CO_2 introduction rate. Data were collected using the Dilor Spectramax program, and processed using a homemade code run with Grams ™ software.

Calibration of Raman spectra

Provided that a calibration was performed, the absolute concentration of a species can be calculated from the area of a spectral peak.[27] The calibration curve for griseofulvin in acetone was constructed from the Raman spectra of six binary solutions, ranging from 3.40 to 33.02 mg_{GRI}/g_{ACE} (or 2.69 to 26.12 mg/mL). The spectral peaks selected to quantify griseofulvin and acetone were centered at Raman shifts of 1620 and 795 cm^{-1}, respectively. Because the griseofulvin peak was partly overlapped by the Raman lines of acetone, the spectrum of pure acetone was extracted from the mixture spectra before integrating the solute peak. Moreover, to account for incidental changes over time of the Raman parameters, which could affect the absolute magnitude of signals, the griseofulvin peak intensity (I_{gri}) was ratioed to the acetone peak intensity (I_{ace}). Therefore, the calibration provided a relationship between the griseofulvin Raman signal represented by I_{gri}/I_{ace} and its concentration in the mixture (CO_2-free content). The CO_2 concentrations were quantified from the area of the peak centered at 1283 cm^{-1}. Raman spectra of pure CO_2 at five pressures and 40°C were used to construct the calibration curve.

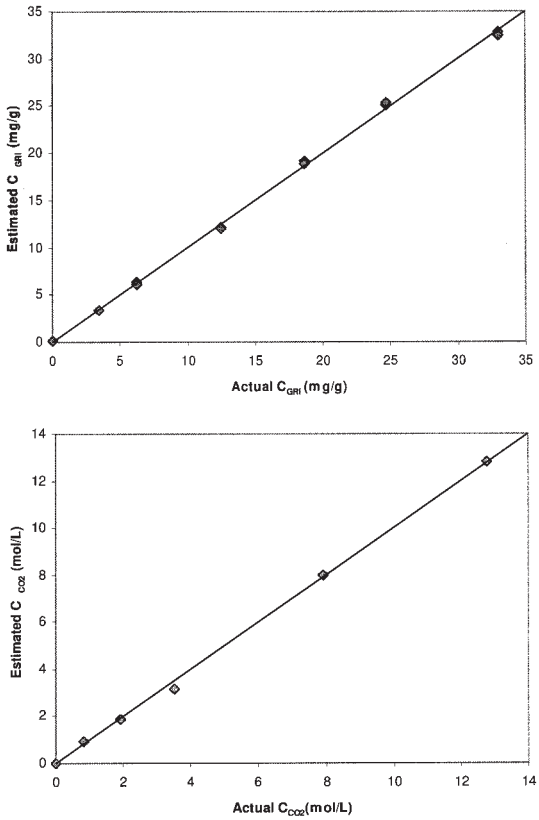

Figure 4. Raman predicted concentrations vs. experimental values for griseofulvin (top plot) and CO_2 (bottom plot).

Figure 4 displays a comparison between the "Raman-predicted values" of GRI and CO_2 concentrations calculated by the peak integration/calibration method, and their corresponding known concentrations. The very good fit over the whole investigated range testifies to the accuracy and performance of the calibrations.

Procedure

Crystallization experiments were carried out at 40°C by adding CO_2 to 100 mL of an initial solution of griseofulvin in acetone (~24 mg/mL in GRI); the stirring was settled at 500 rpm. The procedure consisted of four steps: I. pressurization (Ia: from atmospheric pressure to the cylinder pressure of 6 MPa; Ib: from 6 MPa to the desired final pressure); II. solution discharge; III. crystals drying; IV. depressurization. The solution was first loaded into the vessel at atmospheric pressure and ambient temperature and allowed to stabilize at the operating temperature before the introduction of CO_2. The CO_2 was then gently introduced by means of the inlet metering valve (step Ia), causing an increase of the vessel pressure. To continue the pressurization from the pressure of the CO_2 reservoir to the final desired pressure (step Ib), the CO_2 supply was further ensured by the pump. The system was maintained at the final pressure and upon agitation during a given period of time.

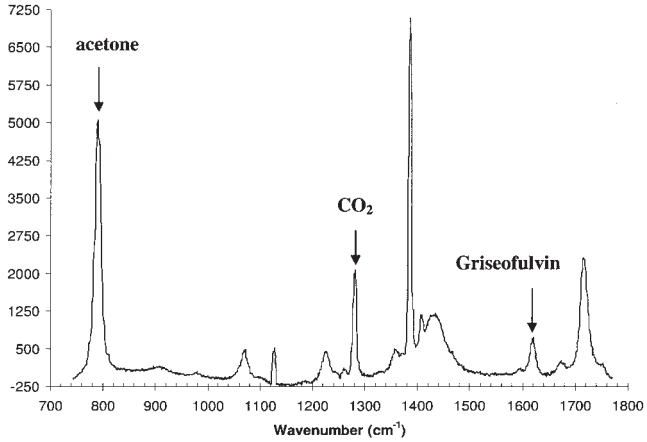

Figure 5. Raman spectrum of the mixture of CO_2–acetone–griseofulvin, collected at a pressure of 4.0 MPa and a temperature of 40°C, during crystallization conditions of Run 1.

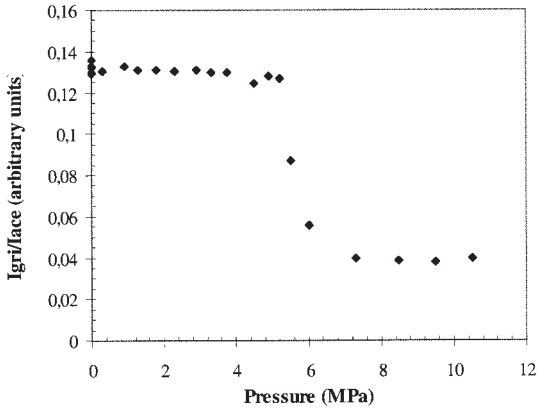

Figure 6. Evolution of the griseofulvin signal expressed as I_{gri}/I_{ace} during the addition of CO_2 to an acetone solution at 30.34 mg/g in conditions of Run 1.

T = 40°C, CO_2 feed rate = 0.12 MPa/min, final pressure of 10 MPa. I_{gri} and I_{ace} are calculated from spectral peaks centered at 1620 and 795 cm^{-1}, respectively.

Then, the solution discharge (step II) was operated under pressure by regulating the exit flow by the exit metering valve and compensating this flow by a feed of fresh CO_2. A flow of pure CO_2 was further maintained to dry the crystals (step III). Depressurization (step IV) was performed by venting the carbon dioxide by the exit line. Crystals were collected on filter and on stirrer for subsequent analysis.

Raman spectra were collected over the whole procedure except during the depressurization step. Because we focus on monitoring crystallization, only spectra recorded during the pressurization step are discussed herein. Spectra were collected at each pressure increment of 0.5 MPa, or, in the case of steady conditions, approximately every 4 min. Figure 5 shows a Raman spectrum acquired during a crystallization experiment. The figure points out the specific peaks that were used to quantify each species, centered at 795, 1283, and 1620 cm^{-1} for acetone, CO_2, and griseofulvin, respectively.

To test the ability of the spectroscopic method to detect and monitor a crystallization induced by supercritical fluids, four experiments were carried out, corresponding to various conditions of crystallization course. Conditions and objectives of the runs are reported in Table 1. Run 1 is based on our standardized procedure for crystallization by CO_2, that is, introduction of CO_2 at a constant rate until a final pressure of 10 MPa that drives the system to a homogeneous solvent–antisolvent mixture. A hold time of 45 min at 10 MPa is settled before starting the discharge step. In Run 2, the continuous addition of CO_2 proceeds until the onset of precipitation. Once the onset is detected, the system is isolated and allowed to regain an equilibrium status. When the Raman signal no longer evolves, fresh CO_2 is further introduced with a consequence of new onset of precipitation. This stepwise procedure continues until a final pressure of 10 MPa. The objective of Run 3 is to study the system evolution after the first burst of precipitation; there is no further addition of CO_2 and subsequent increase of pressure after the first onset of precipitation. Finally, Run 4 is performed in a procedure similar to Run 1, but with a higher CO_2 feed rate.

Analysis of samples

The characteristics of the produced crystals were determined by light and scanning electron microscopy (SEM by Leica S440).

Results and Discussion

Crystallization course vs. pressure

Monitoring of the crystallization course during Run 1 is shown in Figure 6 as a plot of the I_{gri}/I_{ace} ratio vs. pressure. The curve shows three different periods that reflect the events that the solution undergoes. During the first additions of CO_2, the I_{gri}/I_{ace} ratio remains constant. Both the solute and the solvent

Table 1. Experimental Conditions and Runs Objectives*

Run	C_{gri} (mg/mL)	P_f (MPa)	Hold Time at a Given Pressure	CO_2 Addition Rate (MPa/min)	Objectives
1	24.4	10	45 min, at P_f	0.12	Raman feasibility
2	24.3	10	Yes, at P_o and subsequent stepwise pressures	0.10	Inducing several bursts of precipitation
3	24.6	4.8	125 min, at $P_o = P_f$	0.10	System evolution after the first burst of precipitation
4	24.7	10	No	0.45	Testing Raman for monitoring a fast process

*C_{gri}, initial concentration of griseofulvin in acetone; P_f, final pressure; P_o, onset pressure of crystallization. T = 40°C; $V_{initial}$ = 100 mL; stirring rate = 500 rpm.

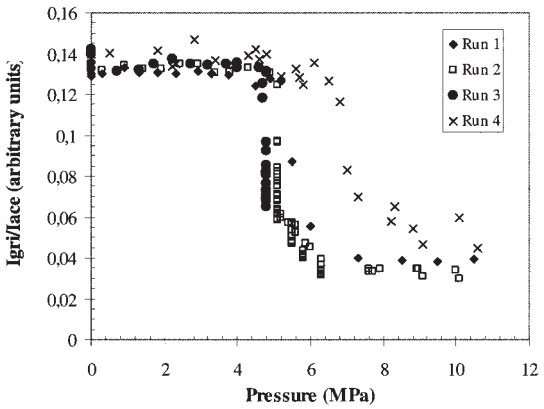

Figure 7. On-line monitoring of griseofulvin signal during the addition of CO_2, for the different experimental conditions.

undergo the same effect, that is a dilution caused by the mixing of the solution with CO_2. As more CO_2 is added, crystallization begins. The solution is depleted in the griseofulvin amount that turns into solid particles and, consequently, the ratio decreases. Finally, an almost constant value is recovered as the pressure is further increased to 10 MPa. This evolution can be discussed in parallel with the qualitative evolution illustrated in Figure 2, and in accordance with the similar qualitative framework proposed earlier.[26,28] The initial concentration of GRI in solution corresponds to 5×10^{-3} mol/mol. The starting point is thus located at point A in Figure 2.

When carbon dioxide is added to the vessel, the solution becomes enriched in CO_2 and, meanwhile, the pressure increases. Once the metastable limit is reached, nucleation and growth start. The mole fraction of CO_2, corresponding to the pressure of precipitation (P_o) of 4.8 MPa, was calculated from the Raman signal and found to be in the 0.6 range. In the specific conditions of Run 1, carbon dioxide addition continues after this first burst of nucleation. Two phenomena compete for the depletion of the solution in solute: new bursts of nucleation upon continuous CO_2 addition and growth of the early nuclei. These two phenomena are not discernable by the I_{gri}/I_{ace} monitoring. After a pressure of 7.4 MPa, the I_{gri}/I_{ace} ratio stabilizes at a value of 0.039. This plateau means that there is neither further significant nucleation nor growth. The pressure of 7.4 MPa corresponds to a CO_2 mole fraction of 0.81. The calculation of the griseofulvin concentration in such solution by the calibration gives a value in the range of 8.7 mg/g. When expressed in mole fraction, it corresponds to 2.5×10^{-4} mol/mol, that is, in the same range of order as the solubility value determined by phase equilibria[23] and reported in Figure 2. Thus, the plateau provides experimental evidence that the system has regained an equilibrium status in terms of crystallization behavior after 7.4 MPa.

The I_{gri}/I_{ace} profiles vs. pressure for the four runs are shown in Figure 7. The final pressure was of 10 MPa in all runs except for Run 3, where there was no further increase of pressure after the onset of crystallization. The pressure of crystallization onset was found to vary with the CO_2 introduction rate, with a value of about 4.8 MPa for experiments performed at 0.11 MPa/min and 6.5 MPa at 0.45 MPa/min. The shift was significant, with respect to the method applied for the onset detection. In this method, the I_{gri}/I_{ace} values of the first period were averaged and a standard deviation was issued. When the ratio changed above this threshold, one considered that crystallization started. Among the four runs, the maximum standard deviation was 0.004 (Run 4) for an averaged I_{gri}/I_{ace} value of 0.139 a.u. (arbitrary unit). This range was found satisfactory for the on-line detection of the crystallization onset because it corresponded to a variation of about 1 mg/g in the solute concentration. Runs 2 and 3 provided a more accurate determination of P_o, given that the system was allowed to sit for a given time once the onset of nucleation was observed. Thus, when crystallization was performed with a CO_2 addition rate of 0.11 MPa/min, the pressure at which first bursts of nucleation were detected was 4.9 ± 0.1 MPa. At a higher feed rate (0.45 MPa/min, Run 4), the onset pressure increased significantly, and the I_{gri}/I_{ace} values also showed greater scattering, even during the earlier period. This behavior may be attributed to a poor mixing between the solution and the CO_2 that consequently drives the system into a situation of nonequilibrium. The efficiency of the mixing process between the solution and the CO_2 affects the local composition of the solvent–antisolvent mixture and, consequently, influence obtaining a condition of supersaturation. On the other hand, Thiering et al.[29] assumed that their system was at equilibrium or well mixed at all stages during the pressurization cycle because the pressurization rates did not significantly affect the conditions of precipitation onset. There is no general rule reported in the literature for the sensitivity of onset pressure with process parameters. This is easily understandable considering the lack of accurate methods for the onset detection (mostly detected visually) and the influence of the mixing—a key variable—with the vessel design, the stirring conditions, the liquor characteristics, and the like[30] that are rarely similar throughout literature.

Crystallization kinetics

The plot of I_{gri}/I_{ace} as a function of time is given in Figure 8 for the four conditions. As before, it depicts the solution events over the duration of the pressurization step; however, the plot vs. time provides an estimate of the overall crystallization rate, time-dependent data that are quite rare for supercritical crystallization processes. That approach is a global method that

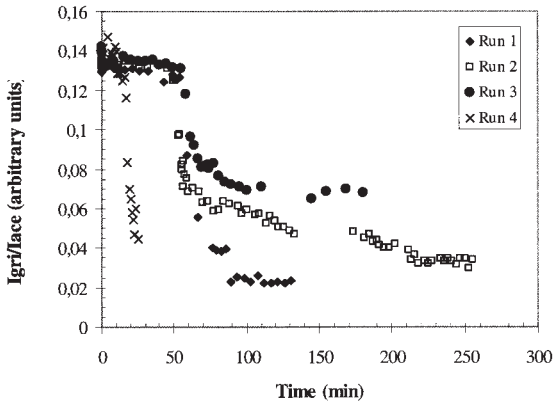

Figure 8. Time change of griseofulvin signal during the addition of CO_2, for the different experimental conditions.

does not allow any distinction between the various mechanisms by which the solution is depleted, that is, the effects of nucleation, growth, aggregation, or attrition are monitored together. Strictly speaking, the decay of the signal depicts a desupersaturation profile of the solution only in conditions of Run 3 because there is no additional introduction of CO_2 after the first onset of precipitation. In the other conditions, it reflects the overall depletion of the solution in solute that occurred both by continuous nucleation arising from the CO_2 feed and by subsequent growth of the older nuclei.

The overall crystallization rate R may be expressed with the general following equation[31]:

$$R = -\frac{dC}{dt} = k\Delta C = k(C_t - C_{eq}) \tag{1}$$

where k is the kinetic constant in min^{-1} for time expressed in min, C_t is the concentration of griseofulvin at time t, and C_{eq} is the concentration at equilibrium. When C_t is expressed in mass ($mg_{gri}/g_{acetone}$), the overall rate R is in mg g^{-1} min^{-1}. With initial conditions defined at the onset of precipitation, the relationship is expressed as

$$\frac{C_t - C_{eq}}{C_{onset} - C_{eq}} = \exp[-k(t - t_{onset})] \tag{2}$$

The calibration curve correlated the concentration to the collected signal; C_{onset} and C_{eq} were determined as averaged values, that is,

- $C_{eq} = (I_{gri}/I_{ace})_f$, the average of values on the final plateau
- $C_{onset} = (I_{gri}/I_{ace})_0$, the average of values on the initial plateau

A linear trend was fitted to $\ln[(C_t - C_{eq})/(C_{onset} - C_{eq})]$ vs. $(t - t_{onset})$, over a period of time that was adjusted to minimize the deviation. Accuracies were of ± 0.7 mg/g for C_{eq} and $\pm 8\%$ for k.

The overall crystallization rates are expressed as

- $R_{run\ 1} = 0.085 \times (C_t - 8.7)$, in the case of a CO_2 feed rate of 0.12 MPa/min and a final pressure of 10 MPa
- $R_{run\ 3} = 0.085 \times (C_t - 15.9)$, in the case of a CO_2 feed rate of 0.10 MPa/min and a final pressure of 4.8 MPa
- $R_{run\ 4} = 0.435 \times (C_t - 10.3)$, in the case of a CO_2 feed rate of 0.45 MPa/min and a final pressure of 10 MPa

There was no relationship for Run 2 because it made no sense to represent a multistep crystallization (stepwise introductions of CO_2 and subsequent hold periods) by a unique overall rate. Experimental data showed that the kinetic constants of runs performed with similar CO_2 introduction rate (Runs 1 and 3) were in the same range, whereas the final equilibrium concentration differed because of a different final pressure. For Run 4, performed at the same final pressure as that of Run 1 but at a feed rate of 0.45 MPa/min instead of 0.12 MPa/min, the kinetic constant was significantly higher, with a value of 0.44 min^{-1} instead of 0.09 min^{-1}. The final concentrations of the two runs also differed. The higher value of 10.3 mg/g obtained in Run 4 still came from the poor mixing of CO_2 and the solution, besides the fact that no hold time was given to the solution to stabilize in an equilibrium status. Although global, these results pointed out and quantified the significant effect of the antisolvent introduction rate upon the overall crystallization kinetics. To interpret more finely the overall crystallization kinetics in terms of nucleation and growth events, it would be necessary to analyze the crystal size distribution (CSD) of the powder, off-line as a first step or in situ as proposed recently by Elvassore et al.[21]

Correlation between Raman signal and results of crystallization

Monitoring the I_{gri}/I_{ace} evolution also enables one to calculate the griseofulvin mass that precipitated during the crystallization course, to quantify the potential gain in continuing the CO_2 addition once the precipitation occurred. The solid content is related to the solute concentration by the simple relationship

$$M^{(t)} = (C_0 - C_t)\, M^0_{acetone} \tag{3}$$

where $M^{(t)}$ represents the mass of griseofulvin that precipitates at time t; $M^0_{acetone}$ is the acetone mass introduced in the vessel; and C_0 and C_t are the griseofulvin concentrations at $t = 0$ (before the introduction of CO_2) and time t, respectively.

In Figures 9a to 9d, the calculated mass of solids generated during the crystallization course (M) is plotted vs. time. To assess the gain of continuing the pressurization after the onset of precipitation, the pressure course of the vessel is also reported. Some mass values appear to drop below zero because the initial concentration C_0 in Eq. 3 was calculated as an average of the I_{gri}/I_{ace} values measured before any introduction of CO_2. The scattering of the I_{gri}/I_{ace} data in Run 4 is of course translated in the mass calculation data, which consequently exhibit significant fluctuations. In conditions of Run 1 (Figure 9a), the onset of crystallization was characterized by an intense burst of solids (from $t \sim 50$ to $t \sim 75$ min) that produced almost 98% of the final mass at a rate of 70 mg min^{-1}. Afterward, the mass evolution was so slow that the additional increase was only 2%. When related to the pressure time course, it is interesting to note that the 98% value was obtained at a pressure of about 7.2 MPa, that is, neither the subsequent addition of CO_2 nor the hold time of 50 min at 10 MPa generated a significant additional mass of crystals. Thus, from a process perspective, it was not necessary to increase the pressure above 7.2 MPa.

Figure 9b allows one to distinguish the time sequences (addition of CO_2 and hold time) that were carried out during Run 2. These sequences lasted from 60 to 7 min. The first precipitation onset, which occurred at 4.9 MPa, again produced a large amount of crystals in 15–20 min, attested by the sharp increase of the curve. This first burst generated nearly 70% of the solids. During the following hold period, the subsequent introductions of CO_2 and their respective hold times induced an additional mass increase of 30%, but at a much lower rate. Between 70 and 220 min, 550 mg of solids were generated, against 1250 mg during the 20-min burst period. As before, there was no gain in pursuing the addition of CO_2 and the pressurization up to 10 MPa because the final content of solids was obtained at 6.3 MPa. The stepwise and the continuous procedure both produced an equivalent amount of crystals, but over a significantly different duration. The stepwise procedure might have compensated in pressure (6.3 instead of 7.2 MPa)

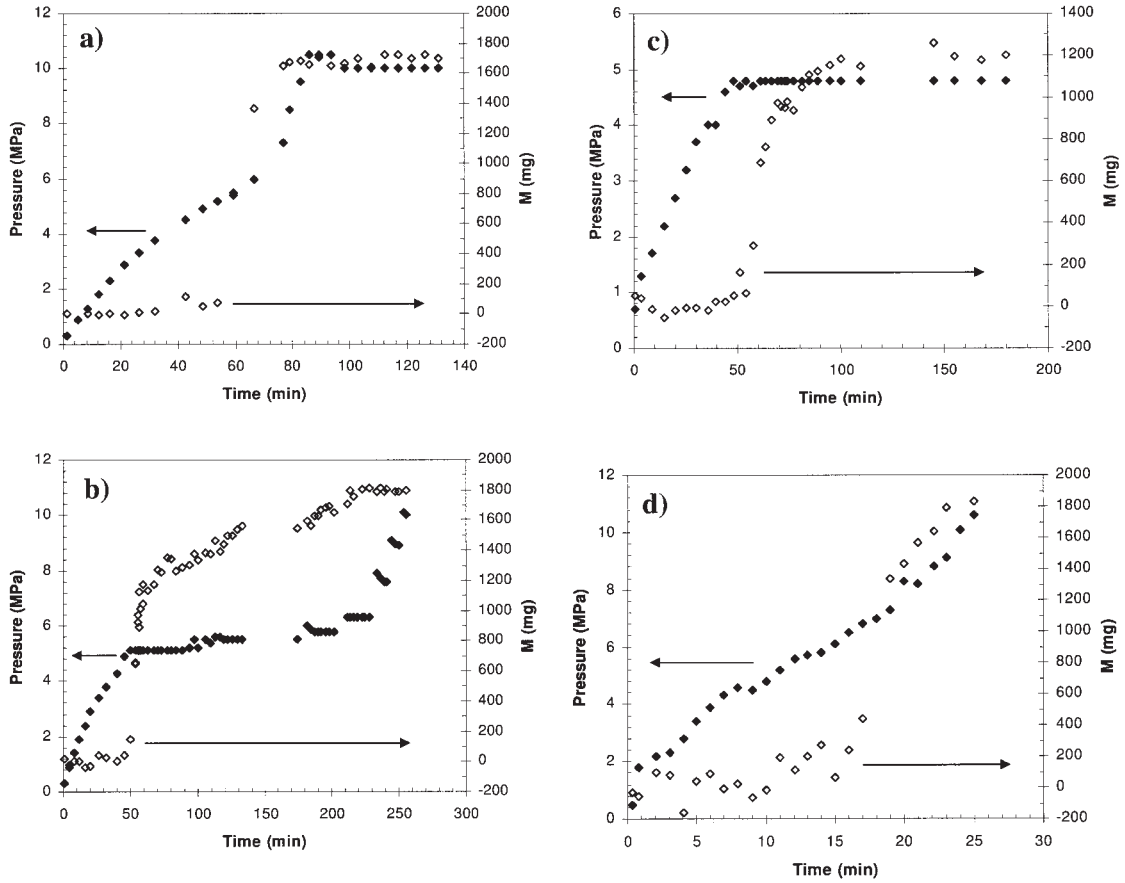

Figure 9. Evolution of the vessel pressure (dark symbols) and of the calculated mass of precipitate (M, open symbols) during the time course of Run 1 (a), Run 2 (b), Run 3 (c), and Run 4 (d).

The mass of precipitated solid was calculated from the I_{gri}/I_{ace} ratio and the calibration curve, according to Eq. 3.

what was lost in time, but a duration of 220 min instead of 75 min was far from an advantage.

In Run 3 (Figure 9c), the hold period was maintained at the onset pressure of about 4.9 MPa. The largest part of solids was produced within 50 min (from $t \sim 50$ to $t \sim 100$ min), with no significant increase of M during the next 80-min period. In Run 4 (Figure 9d), there was no hold time during the crystallization course, so the mass reflected the production of a unique onset of precipitation. During that precipitation, 1800 mg of solids were produced in a short time of nearly 10 min, giving a production rate of 170 mg min^{-1}. The designed set of experiments thus shows that the onset of precipitation is characterized by a fast and important burst of solids with a production of about 70% (Runs 2 and 3) to 98% (Runs 1 and 4) of the final crystals mass in the 25 min that follow the precipitation onset. When time is given to growth (Run 3) or to subsequent minor bursts of nucleation (Run 2), the mass can increase by 30%.

It is interesting to compare the calculated values of the final amount of solids to the experimental ones, obtained by weighing the powder recovered at the end of the experiments (Table 2). Experimental tendencies were in agreement with the expectations from I_{gri}/I_{ace} curves shown in Figure 9. Indeed, calculations have provided evidence of a similar range of solids for Runs 1, 2, and 4, and a lower value for the run stopped at the pressure of 4.8 MPa. The calculated amounts, however, were higher than the experimental ones, with a relative deviation of 11, 17, 23, and 2% for Runs 1 to 4, respectively. Discarding Run 4, which showed a very good agreement, the default in the experimental mass ranged within 200 (Run 1) and 320 mg (Run 2). Several causes can be postulated for the loss of material. One is based on the difficulties in collecting the powder on every part of the vessel. The second is that the suspension of solids at the end of the pressurization step undergoes several subsequent steps before being collected, whereas the one-line monitoring somehow "freezes" the system in a final image. For instance, one step is the discharge of the solution at the vessel bottom and, despite a filter, the smallest particles can escape into the exit line and consequently escape from the collection. Experimental reproducibility should be also taken in account, and was in the 100 mg range for the collected amount. Regard-

Table 2. Calculated and Experimental Amounts of Solids Produced at the End of Four Runs, and Notification of the Experimental Yield, Defined as Experimental Mass over the Initial Content of Griseofulvin

	Run 1	Run 2	Run 3	Run 4
Calculated mass (g)	1.7 ± 0.04	1.8 ± 0.04	1.2 ± 0.05	1.8 ± 0.03
Experimental mass (g)	1.50	1.48	0.92	1.76
Experimental yield (%)	61.4	60.8	37.3	66.6

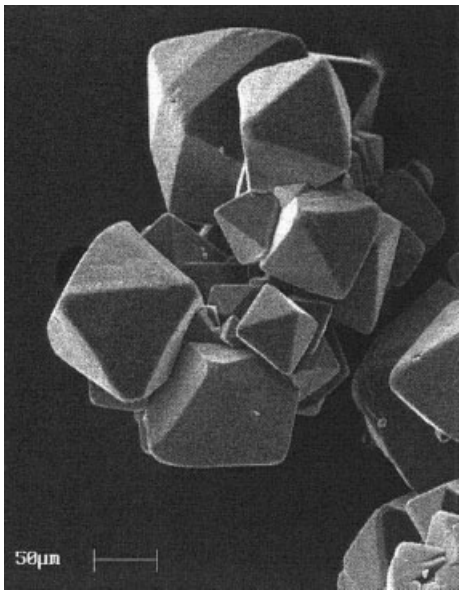

Figure 10. SEM microphotograph of griseofulvin crystals obtained in conditions of Run 2.

ing spectroscopic causes, the maximum deviation in concentration was already mentioned as 1 mg/g. The spectroscopic uncertainties thus represent a mass of 78 mg in griseofulvin. All sources are likely to influence the mass data; however, based on the in situ character of the Raman that is independent of the post-treatment required to collect the powder, and on the lower values of the experimental data, the experimental sources might dominate over the spectroscopic uncertainties.

We now consider results of griseofulvin crystallization, and first, the experimental yield, calculated as the collected mass over the initial amount of griseofulvin introduced into the acetone liquor. The batch crystallization induced by supercritical CO_2 led to the precipitation of 61–67% of the griseofulvin, provided that runs were performed at a final pressure of 10 MPa (Runs 1, 2, and 4). The produced powder consisted of embedded crystals (Figure 10) that showed an individual bipyramidal shape, as already obtained in previous experiments.[22] Crystal dimensions were in the 100 μm range for the base and the edge of pyramids. With such a high degree of agglomeration and in absence of particle size analysis, it seemed ill-advised to discuss the influence of experimental conditions on crystal size. Thus, no conclusions are issued about the best route that combines a high quality of powder and a satisfactory rate or yield of production.

Conclusion

Crystallization induced by the addition of supercritical CO_2 as nonsolvent is gaining importance, although pressurized vessels actually hinder in situ monitoring of the crystallization course. It has been demonstrated in this work that Raman spectroscopy can be used to measure the solute concentration over time in a batch operation and to interpret events during the course of crystallization. The ability to identify specific peaks for solute and solvent allowed for an accurate detection of the onset of precipitation and for the measurement of the depletion profile of the solution as the solute solidified. The accuracy of the detection and of the monitoring was found to be sensitive to the introduction rate of CO_2, mostly because it mirrored the poor mixing efficiency of the CO_2 and the solution at high introduction rate. Furthermore, Raman spectroscopy data provided an estimate of the overall crystallization rate, giving experimental evidence of the predicted scenario of a crystallization induced by supercritical fluid. Compared with experimental data, the anticipated amounts well represented the mass of powder collected at the end of the experiment.

Literature Cited

1. Muzzio FJ, Shinbrot T, Glasser BJ. Powder technology in the pharmaceutical industry: The need to catch up fast. *Powder Technol.* 2002;124:1-7.
2. Steckel H, Pichert L, Müller BW. Influence of process parameters in the ASES process on particle properties of budesonide for pulmonary delivery. *Eur J Pharm Biopharm.* 2004;57:507-512.
3. Raman VI, Palmese GR. Design and characterization of nanoporous polymeric materials via reactive encapsulation of a chemically inert solvent. *Colloid Surf A.* 2004;241:119-125.
4. Wang Y, Dave RN, Pfeffer R. Polymer coating/encapsulation of nanoparticles using a supercritical antisolvent process. *J Supercrit Fluids.* 2004;28:85-99.
5. Schiavone H, Palakodaty S, Clark A, York P, Tzannis ST. Evaluation of SCF-engineered particle-based lactose blends in passive dry powder inhalers. *Int J Pharm.* 2004;281:55-66.
6. JW Mullin. *Crystallization*. 3rd Edition. London: Butterworth-Heinemann; 1993.
7. Yu LX, Lionberger RA, Raw AS, D'Costa R, Wu H, Hussain AS. Applications of process analytical technology to crystallization processes. *Adv Drug Deliv Rev.* 2004;56:349-369.
8. Anderson JE, Moore S, Tarczynski F, Walker D. Determination of the onset of crystallization of N1-2-(thiazolyl)sulphanilamide (sulfathiazole) by UV-Vis and calorimetry using an automated reaction platform; subsequent characterization of polymorphic forms using dispersive Raman spectroscopy. *Spectrochim Acta A.* 2001;57:1793-1808.
9. Uusi-Penttilä M, Berglund KA. Spectroscopic monitoring of environmentally benign antisolvent crystallization. *J Cryst Growth.* 1996;166:967-970.
10. Mougin P, Thomas A, Wilkinson D, White G, Roberts KJ, Herrmann N, Jack R, Tweedie R. On-line monitoring of a crystallization process. *AIChE J.* 2003;49:373-378.
11. Févotte G, Calas J, Puel F, Hoff C. Applications of NIR spectroscopy to monitoring and analysing the solid state during industrial crystallization processes. *Int J Pharm.* 2004;273:159-169.
12. Dunuwila DD, Berglund KA. ATR FTIR spectroscopy for in situ measurement of supersaturation. *J Cryst Growth.* 1997;179:185-193.
13. Schwartz AM, Berglund KA. The use of Raman spectroscopy for in situ monitoring of lysozyme concentration during crystallization in a hanging drop. *J Cryst Growth.* 1999;203:599-603.
14. Schwartz AM, Berglund KA. In situ monitoring and control of lysozyme concentration during crystallization in a hanging drop. *J Cryst Growth.* 2000;210:753-760.
15. Lewiner F, Klein JP, Puel F, Févotte G. On-line ATR FTIR measurement of supersaturation during solution crystallization processes. Calibration and applications on three solute/solvent systems. *Chem Eng Sci.* 2001;56:2069-2084.
16. Févotte G. New perspectives for the on-line monitoring of pharmaceutical crystallization processes using in situ infrared spectroscopy. *Int J Pharm.* 2002;241:263-278.
17. Nattkemper A, Schleiden T, Migliavacca JM, Melin T. Monitoring crystallization kinetics of azelaic acid by in situ FTIR spectroscopy in three-phase systems. *Chem Eng Technol.* 2003;26:881-889.
18. Derdour L, Févotte G, Puel F, Carvin P. Real-time evaluation of the concentration of impurities during organic solution crystallization. *Powder Technol.* 2003;129:1-7.
19. Borissova A, Dashova Z, Lai X, Roberts KJ. Examination of the semi-batch crystallization of benzophenone from saturated methanol solution via aqueous antisolvent drowning-out as monitored in-process using ATR FTIR spectroscopy. *Cryst Growth Des.* 2004;4:1053-1060.
20. Falcon JA, Berglund KA. Monitoring of antisolvent addition crystal-

lization with Raman spectroscopy. *Cryst Growth Des.* 2003;3:947-952.
21. Elvassore N, Parton T, Bertucco A, Di Noto V. Kinetics of particle formation in the gas antisolvent precipitation process. *AIChE J.* 2003; 49:856-868.
22. De Gioannis B, Jestin P, Subra P. Morphology and growth control of griseofulvin recrystallized by compressed carbon dioxide as antisolvent. *J Cryst Growth.* 2004;262:519-526.
23. De Gioannis B, Vega-González A, Subra P. Antisolvent and cosolvent effect of CO_2 on the solubility of griseofulvin in acetone and ethanol solutions. *J Supercrit Fluids.* 2004;29:49-57.
24. Tur KM, Ch'ng H-S, Baie S. Use of bioadhesive polymer to improve the bioavailability of griseofulvin. *Int J Pharm.* 1999;148:63-71.
25. Subra P, Jestin P. Powders elaboration in supercritical media: Comparison with conventional routes. *Powder Technol.* 1999;103:2-9.
26. Müller M, Meier U, Kessler A, Mazzotti M. Experimental study of the effect of process parameters in the recrystallization of an organic compound using compressed carbon dioxide as antisolvent. *Ind Eng Chem Res.* 2000;39:2260-2268.
27. Rice SF, Hunter TB, Rydén ÅC, Hanush RG. Raman spectroscopic measurement of oxidation in supercritical water. 1. Conversion of methanol to formaldehyde. *Ind Eng Chem Res.* 1996;35:2161-2171.
28. Gallagher PM, Coffey MP, Krukonis VJ. Gas antisolvent recrystallization of RDX: Formation of ultra-fine particles of a difficult-to-comminute explosive. *J Supercrit Fluids.* 1992;5:130-142.
29. Thiering R, Dehghani F, Dillow A, Foster NR. The influence of operating conditions on the dense gas precipitation of model proteins. *J Chem Technol Biotechnol.* 2000;75:29-41.
30. Nere N, Patwardhan W, Joshi J. Liquid-phase mixing in stirred vessels: Turbulent flow regime. *Ind Eng Chem Res.* 2003;42:2661-2698.
31. Cai J-G, Liao X-C, Zhou Z-Y. Microparticle formation and crystallization rate of HMX using supercritical carbon dioxide antisolvent recrystallization. *Proceedings of the 4th International Symposium on Supercritical Fluids at Sendai, Japan*. Nancy, France: ISASF; 1997: 23-29.

Manuscript received July 13, 2005, and revision received Sept. 16, 2005.